ELSEVIER

Cement & Concrete Composites 24 (2002) 229–241

Cement & Concrete Composites

www.elsevier.com/locate/cemconcomp

A finite element assessment of flexural strength of prestressed concrete beams with fiber reinforcement

S.K. Padmarajaiah [a], Ananth Ramaswamy [b,*]

[a] *NAL Bangalore - 560 017, India*

[b] *Civil Engineering Department, Indian Institute of Science, Bangalore 560 012, India*

Received 10 May 2000; accepted 24 May 2001

Abstract

This paper presents an assessment of the flexural behavior of 15 fully/partially prestressed high strength concrete beams containing steel fibers investigated using three-dimensional nonlinear finite elemental analysis. The experimental results consisted of eight fully and seven partially prestressed beams, which were designed to be flexure dominant in the absence of fibers. The main parameters varied in the tests were: the levels of prestressing force (i.e, in partially prestressed beams 50% of the prestress was reduced with the introduction of two high strength deformed bars instead), fiber volume fractions (0%, 0.5%, 1.0% and 1.5%), fiber location (full depth and partial depth over full length and half the depth over the shear span only). A three-dimensional nonlinear finite element analysis was conducted using ANSYS 5.5 [Theory Reference Manual. In: Kohnke P, editor. Elements Reference Manual. 8th ed. September 1998] general purpose finite element software to study the flexural behavior of both fully and partially prestressed fiber reinforced concrete beams. Influence of fibers on the concrete failure surface and stress–strain response of high strength concrete and the nonlinear stress–strain curves of prestressing wire and deformed bar were considered in the present analysis. In the finite element model, tension stiffening and bond slip between concrete and reinforcement (fibers, prestressing wire, and conventional reinforcing steel bar) have also been considered explicitly. The fraction of the entire volume of the fiber present along the longitudinal axis of the prestressed beams alone has been modeled explicitly as it is expected that these fibers would contribute to the mobilization of forces required to sustain the applied loads across the crack interfaces through their bridging action. A comparison of results from both tests and analysis on all 15 specimens confirm that, inclusion of fibers over a partial depth in the tensile side of the prestressed flexural structural members was economical and led to considerable cost saving without sacrificing on the desired performance. However, beams having fibers over half the depth in only the shear span, did not show any increase in the ultimate load or deformational characteristics when compared to plain concrete beams. © 2002 Published by Elsevier Science Ltd.

Keywords: Flexural strength; Partial depth fibers; Load–deflection response; fully/partially prestressed beams; High strength fiber reinforced concrete; Finite element analysis; Fiber bond-slip

1. Introduction

High-strength concrete is preferred in prestressed concrete members, as the material offers high resistance in compression. In the anchorage zone the bearing stresses being higher, high strength concrete is invariably preferred to minimize the costs. High strength concrete is less liable to shrinkage cracks, has a higher modulus of elasticity and a reduced creep strain, resulting in smaller losses in the applied initial prestress. High strength together with the desired ductility may be achieved by introducing small discrete fibers into the concrete matrix.

Investigations have been conducted to assess the suitability of the use of steel fiber reinforcements together with normal concrete containing conventional reinforcement [2,4–9] to improve the structural behavior. The main objective of most of these studies have been the estimation of ultimate strength and the behavior of beams having steel fibers along with the conventional reinforcement over the entire loading. However, reported research efforts on the behavior of fiber reinforced high strength concrete in the area of prestressed and conventionally reinforced concrete structures is limited. The few research studies on the use

* Corresponding author. Fax: +91-80-3600-404.
E-mail address: ananth@civil.iisc.ernet.in (A. Ramaswamy).

0958-9465/02/$ - see front matter © 2002 Published by Elsevier Science Ltd.
PII: S0958-9465(01)00040-3

Nomenclature

Notations

A_e	cross-sectional area of concrete element
A_f	cross-sectional area of fiber
a	shear span
E_c	initial tangent modulus of fiber reinforced concrete
f_c	uniaxial ultimate cylindrical compressive strength plain concrete
f_{cf}	uniaxial cylindrical compressive strength of SFRC
f_{cb}	biaxial compressive strength
f_{ck}	cube compressive strength of plain concrete
f''_{ck}	cube strength of plain concrete at transfer of prestress
f_{ckf}	cube compressive strength of fiber reinforced concrete
f_{spcf}	split cylinder strength SFRC
f_t	uniaxial ultimate tensile strength of plain concrete
f_1	ultimate compressive strength for a state of biaxial compression superimposed on σ_h stress
f_2	ultimate compressive strength for a state of uniaxial compression superimposed on σ_h stress
P	peak load
$(P_c)_{expt}$	experiment cracking load
$(P_u)_{expt}$	experiment ultimate load
$(P_c)_{FEM}$	cracking load from FEM
$(P_u)_{FEM}$	ultimate load from FEM
v_r^1	stiffness multiplier for cracked tensile condition
W	applied load
α^1	fiber orientation factor
β_t	shear retention factor for open crack
β_c	shear retention factor for closed crack
δ	central deflection
v_{cf}	Poisson's ratio for SFRC
σ_h	hydrostatic ambient state of stress

of fibers in prestressed reinforced concrete include a study on the behavior of SFRC prestressed beams under impact [10] and some shear studies on normal and medium strength partially prestressed fiber reinforced concrete beams [11–14]. Torsional behavior of fiber reinforced prestressed concrete have also been studied [15–17].

Few studies have been found in the literature, that use the concept of inclusion of fibers over partial depth of the beam in the area of normal strength concrete without tensile steel [18,19]; Rahimi and Kelser (mortar matrix) [20]. Swamy and Al-Ta'an [4] studied the use of partial depth of fiber in concrete beams having conventionally reinforcements. As steel fibers form quite an expensive constituent material in SFRC, it is of importance to determine ways and means of using the fibers in an optimal way. The authors have not been able to locate any previous studies on the flexural behavior of prestressed concrete specimens where fibers were distributed over only a partial depth of the beam.

An excellent state of the art report ASCE [21] in the area of finite elements analysis of reinforced concrete structures presents a complete review of the factors which should be considered for the analysis of concrete structures. These factors range from models for the stress strain response for concrete (nonlinear elastic, elasto-plastic, etc.), failure surface for concrete (e.g. five parameter model of Willam and Warnke [25]), simulation of cracks (discrete and smeared), simulation of reinforcement (discrete, embedded, and smeared), and stress strain models for the reinforcement (eq. bilinear elastic hardening plastic). Methods of including concrete steel interface bond slip and tension stiffening models and sophistication in the crack interface models have also been discussed in this state of the art report ASCE [21]. Numerous general purpose computer programs are available for the analysis of reinforced concrete structures and to a much lesser extent, for prestressed concrete systems. However, modeling the effect of fibers on concrete, fiber bond/slip, and the bridging effects across cracks has still not been taken into account in FE analysis of SFRC structures in any of these programs.

Thus the major emphasis of the present study was to determine flexural strength of high strength fiber reinforced concrete prestressed members. In the finite element study using ANSYS [1], to simulate the effect of steel fibers in a concrete matrix its behavior has been decomposed into two components. Firstly, the multiaxial stress state in concrete due to the presence of fibers has been simulated by modifying the parameters used to describe the concrete failure surface and stress–strain properties. Secondly, the fibers along the beam length have also been modeled as truss elements explicitly in order to capture the crack propagation resistance through bridging action. The prestressing wires (with initial pre-strain), conventional steel and stirrups have also been modeled as truss elements. Tension stiffening and bond slip between concrete and reinforcement (fiber, prestressing wire, and rebars) have been considered in this model using linear springs.

2. Experimental details

2.1. Specimen and test variables

All the beams (eight fully and seven partially prestressed) had the same plain concrete strength of 65 MPa. The variables in the test specimen were: amount of prestressing, volume fraction of trough (similar to hooked end) shape steel fibers (0%, 0.5%, 1.0%, and 1.5%) with constant fiber aspect ratio of 80, and fiber locations.

Portland cement, crushed granite aggregate (12.5 mm size and down), and clean river sand were used in the specimen. The design mix employed in the specimen was arrived at by a trial and error process. For an assumed water cement ratio (w/c) of 0.5 the trial mix of concrete developed as per the procedure outlined in IS handbook SP: 23 [22] and Nagaraj and Bhanu [23], was used to cast cube specimen which were tested in compression and hence led to the determination of the final mix proportion. The final design mix used to cast all the beams were 1:1.128:1.385 (cement:fine aggregate:coarse aggregate) with a w/c ratio of 0.36 in order to achieve a 28 day strength of 65 MPa in plain concrete.

The test programs consisted of fabricating and testing 15 beams having identical rectangular cross-section of 105×240 mm having a length of 2200 mm, under four point loads as shown Fig. 1(a). The strain gauges, 15 mm in gauge length, having a resistance of 118–124 Ω and a gauge factor of 2.14, were insulated and adequately water proofed before concreting. Each wire was tensioned up to a load of 3.6 tonnes which produced a total applied prestress of 3670.67 MPa (4×917.67) in fully prestressed beams and 1835.34 MPa in partially prestressed beams (2×917.67). The prestressing force was transferred by cutting the wires using welding after 6–11 days of the curing of concrete. Thereafter, the prestressed specimens were removed from the pretensioning bed and cured under wet gunny bags for 28 days. All the prestressed beams were tested at the age of 29–30 days. Fig. 1(a) and (b) shows the detailed loading arrangements along with demec points locations. Fig. 1(c)–(j) shows the cross-sectional details of the beam specimens. Table 1 gives the details for each of the specimen at transfer and at testing.

The loads were applied in small increments and at every increment of loading, the deflections were measured using dial gauge of least count 0.01 mm, and the concrete surface strain at each section (Fig. 1(b)) marked as A, B, C, D, and E on each face were measured using a 200 mm gauge length demec gauge, having a least count of 0.79×10^{-5}. The specimen was carefully observed for cracks and its growth at every increment and the load at the appearance of the first cracks was noted. Thereafter, the appearance and progress of all

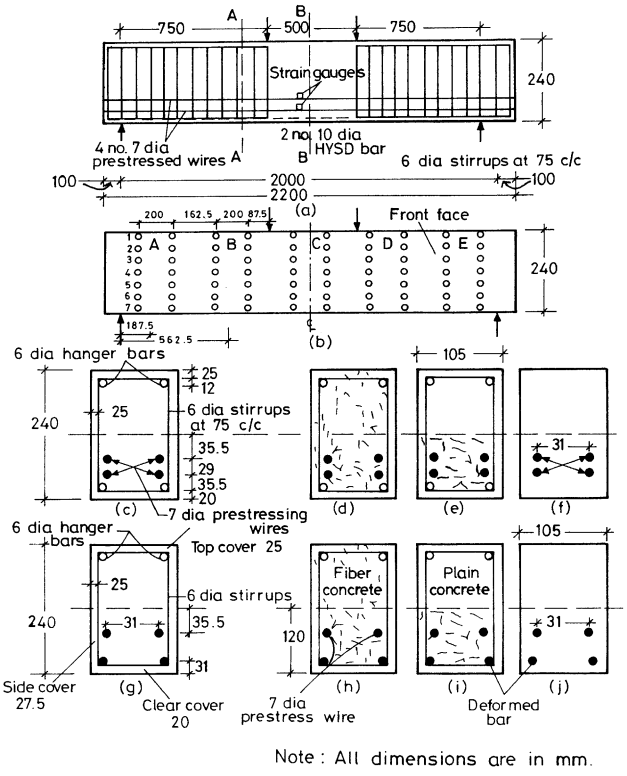

Fig. 1. (a) The set-up, (b) Strain Rosette details, (c) C/S details for specimen A-FP/f0-0, (d) C/S details for specimen A-FP/f0-5, A-FP/f1-0, and A-FP/f1-5; (e) C/S details for specimen A-FPhf/f1-0, B-FPhf/f1-5 having partial depth FRC over full length of the Beam; (e) and (f) C/S details for specimens A-FPhs/f1-0 and A-FPhs/f1-5 having partial depth FRC over only shear span. (g) C/S details for partially prestressed beam specimen A-PP/f0-0; (h) C/S details for specimen A-PP/f1-0 and A-PP/f1-5; and (i) and (j) C/S details for specimen having fibers only in the shear span A-PPhs/f1-0 and A-PPhs/f1-5.

cracks was carefully marked out after each increment. At failure, the ultimate load and mode of failure were noted. After testing, the pattern of cracks were transferred to a graph sheet to get the spacing of crack at different stages of loading. The companion cube strength and flexural prisms were tested on the same day as the corresponding test of the prestressed beams.

3. Finite element modelling

Fig. 2(a) shows the FE model used for the analysis of fully/partially prestressed specimens. Taking advantage of symmetry only half the beam was modelled using concrete SOLID65 three-dimensional elements [1]. The mesh consisted of 16 concrete elements along the length, eight elements over the depth and three elements across the width. The mesh employed for the study had element length of 75 mm in shear span, where as 50 mm element size was used in the flexure zone. The cross-sectional

Table 1
Summary of beam details and summary of test and FEM results

Sl	Beam	v_f	At transfer		At testing			At cracking				At ultimate			
			Age (days)	f''_{ck} (MPa)	Age (days)	f_{ckf} (MPa)	f_{spcf} (MPa)	$(P_c)_{expt}$ (kN)	% Incr	$(P_c)_{FEM}$ (kN)	% Incr	$(P_u)_{expt}$ (kN)	% Incr	$(P_u)_{FEM}$ (kN)	% Incr
1	A-FP/f0-0	0.00	9	48.40	29	64.96	5.23	55.43	–	53.13	–	96.99	–	90.45	–
2	A-FP/f0-5	0.50	9	48.39	29	65.62	5.93	59.94	8.00	54.15	2.00	104.21	7.45	97.50	7.80
3	A-FP/f1-0	1.00	7	50.36	29	66.71	8.62	60.00	8.50	57.50	8.20	112.40	15.85	103.50	16.09
4	A-FP/f1-5	1.50	7	50.36	29	68.02	10.13	64.46	16.40	60.30	13.50	117.31	20.97	110.50	22.17
5	A-FPhf/f1-0	1.00	11	54.36	29	66.71	8.21	58.14	5.00	55.13	4.00	106.92	10.25	102.84	13.70
6	A-FPhf/f1-5	1.50	11	54.36	29	67.36	10.03	64.46	16.29	60.53	14.00	110.54	14.00	106.50	17.75
7	A-FPhs/f1-0	1.00	11	54.36	29	66.71	8.21	56.87	3.00	54.16	2.50	99.24	2.50	93.50	3.10
8	A-FPhs/f1-5	1.50	11	54.36	29	67.36	10.03	57.95	4.50	54.90	5.00	101.47	5.00	97.51	4.30
9	A-PP/f0-0	0.00	6	47.09	30	65.18	5.31	42.78	–	42.51	–	91.66	–	87.20	–
10	A-PP/f1-0	1.00	6	47.09	30	66.05	8.79	50.91	18.18	47.56	11.88	105.12	14.73	100.50	15.25
11	A-PP/f1-5	1.50	7	53.48	30	68.02	10.35	55.42	28.67	49.21	15.76	109.63	19.66	105.54	21.03
12	A-PPhf/f1-0	1.00	7	49.85	29	66.27	8.21	46.39	15.37	47.02	10.61	101.50	10.80	97.89	13.41
13	A-PPhf/f1-5	1.50	7	53.48	29	68.02	10.35	55.43	28.67	48.77	14.73	105.12	14.73	102.23	17.24
14	A-PPhs/f1-0	1.00	7	49.85	29	66.27	8.21	46.39	7.71	43.55	2.50	96.99	5.90	91.50	4.93
15	A-PPhs/f1-5	1.50	7	53.48	30	68.23	10.35	46.39	7.71	44.05	3.60	99.24	8.32	94.32	8.16

% Incr = Percentage increase of strength with respect to control beam specimen.

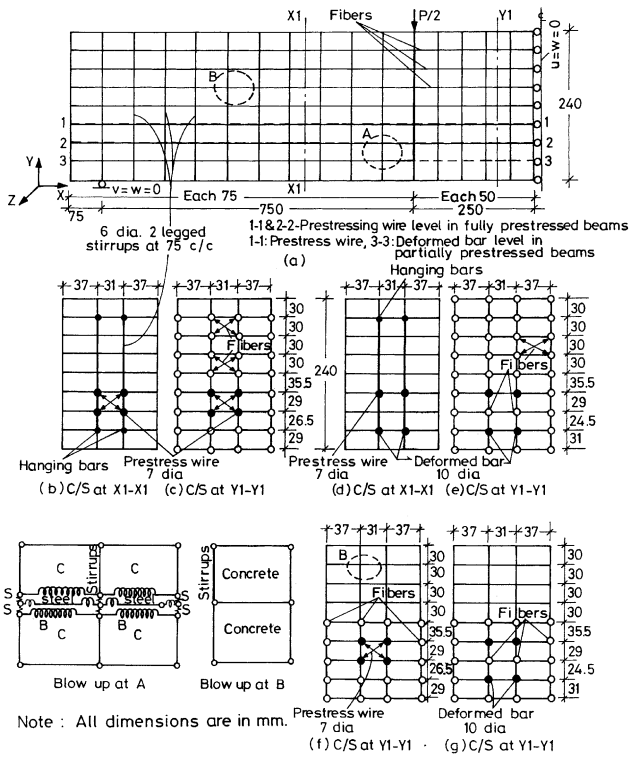

Fig. 2. (a) FE model for fully/partially prestressed SFRC beam specimens, (b) cross-sectional details for fully prestressed plain concrete beam specimens, (b) and (c) cross-sectional details for full depth SFRC fully prestressed beam specimen, (d) cross-sectional details for partially prestressed plain concrete beam specimens, (d) and (e) cross-sectional details for full depth SFRC partially prestressed beam specimen, (f) partial depth SFRC fully prestressed beam specimens, (g) partial depth SFRC partially prestressed beam specimens.

details of the elements width, and height used at various locations is shown in Fig. 2(b)–(g).

To simulate the behavior of prestressing wires and deformed bars, LINK8 (truss) element from the ANSYS 5.5 [1] library have been used. The interface behavior between the concrete and reinforcement (prestressing wire and reinforcing bar) has been modelled using COMBIN14 (spring) elements, with different properties to capture the effect of bond, bond-slip and peel-off. Fig. 2 shows the details in blow up 'A' for fully prestressed beams and blow up 'B' shows the details of bond slip spring elemental details for partially prestressed beams. Each prestressing/deformed bar LINK8 contains two springs at each end (COMBIN14 elements), one acting perpendicular to the prestressing/bar steel and one acting parallel to prestressing/bar steel, as shown in the Fig. 2. Every short segment of the LINK8 acts as a prestressing wire or reinforcement bar. The mild steel stirrups and stirrups hangers in the flexure zone have also been modeled using truss (LINK8) elements, assuming perfect bond between these elements with concrete.

The finite element mesh details for the case of fiber reinforced beams has also been shown in Fig. 2. All the flexure critical beams having fiber over the full depth or partial depth were observed to have failed in flexure with fiber pull-out across the cracks, rather than through yielding of the fiber. In order to simulate the effect of steel fibers in a concrete matrix, its behavior has been decomposed into two components. The multiaxial state of stress in concrete due to the presence of fiber has been simulated by modifying the failure surface of concrete and its stress strain response as indicated in the material property section later in this paper. The bridging action of fibers resisting crack propagation has been modelled using three-dimensional LINK8 (truss) elements explicitly. The fraction of the entire volume of the fiber present along the longitudinal axis of the prestressed beams alone has been modeled explicitly, in the flexure zone. In the case of beams containing fibers over partial depth along the full length, the fibers were modeled only over half the depth in the flexure zone (fibers in the shear span were ignored). Likewise, no fibers were modeled in the case of beams having fibers only over half depth in the shear span, as fibers were not expected to contribute to pulling across the crack in the flexure zone in these specimen. The effect of tension stiffening and bond-slip at the interface between these fiber elements and concrete elements have also been simulated using COMBIN14 (linear springs) elements with appropriate properties to capture the effects of bond, bond-slip and peel off.

Selection of element size is an important factor in the finite element analysis of concrete structures. It has been reported by Bazant and Oh [24], that the smallest element dimension in an FE model is controlled by the size of the coarse aggregate used i.e, 12.5 mm used in the present study. It has been further argued by Bazant and Oh [24] that it makes no sense to use higher order shape functions with such small elements. The mesh employed in this study was arrived at taking into account these considerations along with the computational effort involved.

3.1. Material properties

3.1.1. Concrete elements

Table 2 shows the basic material properties used in FE analysis. The failure criterion for concrete due to multiaxial state of stress used in the study was the Willam and Warnke [25] five parameter model ANSYS 5.5 [1]. Two input parameters viz., the uniaxial tensile strength (f_t) and the ultimate uniaxial compressive strength (f_c) were obtained from average values of the modulus of rupture test and the compressive cylinder test conducted in this study for plain concrete (Table 2). For plain concrete elements the remaining three failure

Table 2
Concrete material properties used in FE analysis for flexure critical prestressed beam specimens

Sl	Beam	v_f	f_{cf} (MPa)	f_t (MPa)	σ_h (MPa)	f_{cb} (MPa)	f_1 (MPa)	f_2 (MPa)	β_t	β_c	v'_r	E_c (GPa)	v_c
1	A-FP/f0-0	0	58.01	5.23	100.48	69.81	84.11	100.07	0.25	0.7	0.45	40.58	0.25
2	A-FP/f0-5	0.5	58.6	5.93	101.49	70.32	98.09	191.04	0.4	0.75	0.6	41.55	0.26
3	A-FP/f1-0	1	59.57	8.62	103.18	98.29	778.64	458.03	0.55	0.8	0.9	42.53	0.28
4	A-FP/f1-5	1.5	60.74	10.13	105.2	100.22	1032.58	607.4	0.65	0.9	0.95	43.5	0.29
5	A-FPhf/f1-0	1	59.57	8.21	103.18	98.29	778.64	458.03	0.55	0.8	0.9	42.53	0.28
		–[a]	58.01	5.23	100.48	69.81	84.11	100.07	0.25	0.7	0.45	40.58	0.25
6	A-FPhf/f1-5	1.5	60.15	10.03	104.19	99.25	1022.55	601.5	0.65	0.9	0.95	43.5	0.29
		–[a]	58.01	5.23	100.48	69.81	84.11	100.07	0.25	0.7	0.45	40.58	0.25
7	A-FPhs/f1-0	1	59.57	8.21	103.18	98.29	778.64	458.03	0.55	0.8	0.9	42.53	0.28
		–[a]	58.01	5.23	100.48	69.81	84.11	100.07	0.25	0.7	0.45	40.58	0.25
8	A-FPhs/f1-5	1.5	60.15	10.03	104.19	99.25	1022.55	601.5	0.65	0.9	0.95	43.5	0.29
		–[a]	58.01	5.23	100.48	69.81	84.11	100.07	0.25	0.7	0.45	40.58	0.25
9	A-PP/f0-0	0	58.21	5.31	100.82	69.85	84.41	100.41	0.25	0.7	0.45	50.58	0.25
10	A-PP/f1-0	1	58.99	8.79	102.17	97.33	771.06	453.57	0.55	0.8	0.9	42.53	0.28
11	A-PP/f1-5	1.5	60.74	10.35	105.2	100.22	1032.58	607.4	0.65	0.9	0.95	43.5	0.29
12	A-PPhf/f1-0	1	59.18	8.21	102.5	97.65	773.54	455.04	0.55	0.8	0.9	42.53	0.28
		–[a]	58.01	5.23	100.48	69.81	84.11	100.07	0.25	0.7	0.45	40.58	0.25
13	A-PPhf/f1-5	1.5	60.74	10.35	105.2	100.22	1032.58	607.4	0.65	0.9	0.95	43.5	0.29
		–[a]	58.01	5.23	100.48	69.81	84.11	100.07	0.25	0.7	0.45	40.58	0.25
14	A-PPhs/f1-0	1	59.18	8.21	102.5	97.65	773.54	455.03	0.55	0.8	0.9	42.53	0.28
		–[a]	58.01	5.23	100.48	69.81	84.11	100.07	0.25	0.7	0.45	40.58	0.25
15	A-PPhs/f1-5	1.5	60.93	10.35	105.54	100.53	1035.81	609.3	0.65	0.9	0.95	43.5	0.29
		–[a]	58.01	5.23	100.48	69.81	84.11	100.07	0.25	0.7	0.45	40.58	0.25

[a] Material properties used for plain concrete element zone.

parameters viz., biaxial compressive strength (f_{cb}), ultimate compressive strength for a state of biaxial compression (f_1) superimposed on a hydrostatic stress state and an ultimate compressive strength for a state of uniaxial compression (f_2) superimposed on a hydrostatic stress state (σ_h) were assumed to be the default values of ANSYS 5.5 [1]. These default values have been set so as to represent the Willam and Warnke [25] surface which has been validated for a large number of tests of plain concrete elements under different stress states. For SFRC elements, the values of f_t, and f_{cf} have been taken from the present test results for different fiber volume fractions (Table 2). The biaxial compressive strength of SFRC (f_{cb}) was obtained from the experimental results of Yin et al. [26]. The remaining two parameters f_1 and f_2 were determined by a trial and error process for a modified Willam and Warnke [25] failure surface accounting for the presence of fibers based on the work of Chuan et al. [3]. Chuan et al. [3] have proposed modified coefficients for the equations representing the tensile and compressive meridians of the Willam and Warnke [25] failure surface accounting for the volume fraction of fibers. In this study the values of f_1 and f_2 for a assumed hydrostatic ambient state of stress ($\sigma_h = \sqrt{3}f_{cf}$) were obtained from a trial and error process such that these two values corresponded to points lying on the failure surface for each given fiber volume fraction. These values of f_1 and f_2 have been tabulated in Table 2 for the given volume fraction of fibers. The crack interface shear transfer coefficient (β_t) for open cracks was assumed to range from 0.1 to 0.5 while for closed cracks the shear transfer coefficient (β_c) was assumed to range from 0.7 to 0.9 as shown in Table 2. The higher range of values were assumed for SFRC as it was expected that the fibers would contribute significantly to shear transfer across a crack.

3.2. Fibers

The effectiveness of steel fibers in increasing the tensile strength of the concrete, at least partially, depends on the number of fibers per unit cross-sectional area of concrete. The fraction of the entire volume of the fiber present along the longitudinal axis of the beams alone was modeled explicitly as it was expected to contribute to the mobilization of forces required to sustain the applied loads after concrete cracking and provide resistance to crack propagation. The number of fiber per unit area along the beam length was calculated in this study, based on the probability approach given by Parviz and Lee [27]. The equations given in the literature [27,28] to predict the number of fibers per unit cross-sectional area of concrete are of the form:

$$N_f = \alpha^1 \frac{v_f}{A_f}, \tag{1}$$

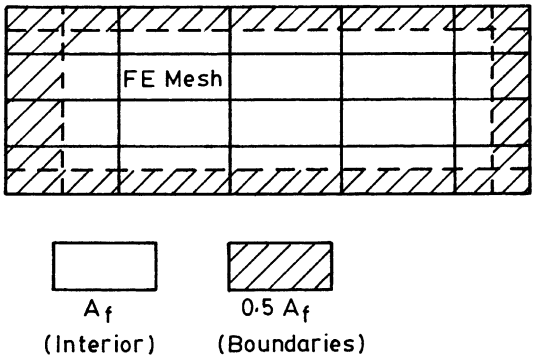

Fig. 3. Tributary area employed to compute the amount of fibers between FE elements.

where α^1 is the orientation factor which ranges from 0.41 to 0.82 [4,27,29].

Orientation of these fibers in concrete and consequently the number of fibers per unit cross-sectional area is influenced not only by the boundaries restricting the random orientation of fibers, but also by the fact that the fibers tend to settle down and reorient in horizontal planes when the fiber concrete matrix is vibrated during casting. As a result of vibration, the random orientation of fibers in concrete moves away from a three-dimensional condition to a two-dimensional condition. Hence, the value α^1 was taken based on the 2-D orientation of the fibers as equal to 0.645 (average value of 0.55–0.74 proposed by Parviz and Lee [27]). Thus the number of fibers per finite element is given by:

$$A_f = \alpha^1 v_f A_e, \tag{2}$$

were A_e is the cross-sectional area of a concrete element. Thus knowing α^1, the number of fiber between each element was calculated for each finite element mesh shown in Fig. 3. The elements lying at the boundary carry half of the area of fibers used in interior of the FE mesh. The nonlinear material behavior of the fibers (Fig. 4) was inputed into the ANSYS program as a rate-independent material nonlinear stress strain curve.

3.3. Prestressing wires and deformed bars

In the present study, the prestressed wire and deformed bar (in the partially prestressed beams), stirrups, and stirrups hanging bar were simulated using LINK8 truss elements. The points on the nonlinear material properties of the stress strain curve for prestressed wire and deformed bar were input into the ANSYS modeling as shown in Fig. 4 obtained from actual tests in this study. The effect of prestress was modeled as an effective initial prestrain applied on each prestress wire truss element uniformly.

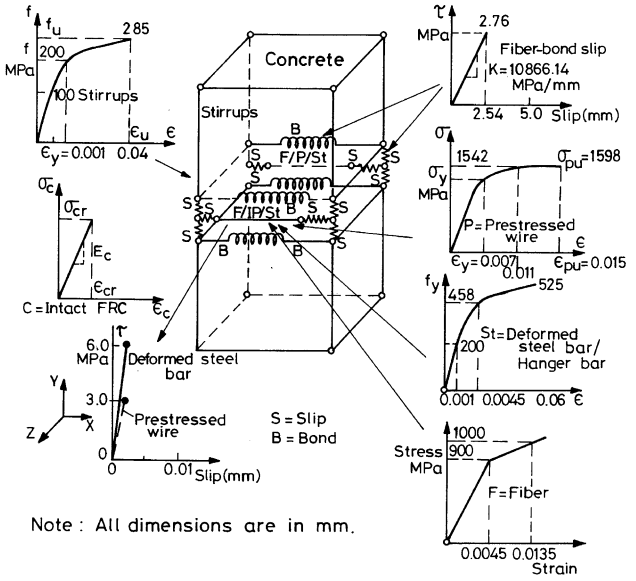

Fig. 4. Rheological representation of a prestressed fiber reinforced concrete element.

3.4. Bond

In the present study, the inter-facial bond between concrete and steel elements (fiber/prestress wire/deformed bar) was simulated using COMBIN14 (linear springs) elements in the ANSYS 5.5 [1] elements library, with appropriate properties to capture the effects of bond, bond-slip and peel off. The interface bond stiffness between concrete and fibers were obtained from the bond stress versus slip curve (linear) test data of George Nammer and Naaman [30] (Fig. 4) without cut-off. As no experimental data has been reported in the literature for the bond between smooth prestressing wire and the concrete, in this study the bond between smooth mild steel bar and concrete has been taken as the bond between prestress wire and concrete. The bond stress is mainly effected by surface characteristics and thus is the same for both prestress wire and smooth mild steel bar. Hence the spring stiffness at the interface between concrete and prestressing wire was obtained from the bond stress verses slip curve shown from the test data of Edwards and Yannopoulos [31] (Fig. 4). Where as in the case of deformed bar, bond between deformed bars and concrete was also obtained from the test data of Edwards and Yannopoulos [31] (Fig. 4). Based on test results, Spencer et al. [32] concluded that in the pre-peak region, the bond stress slip relation between deformed bar in fiber concrete was almost the same as that in plain concrete and due to effect of fibers the bond-slip curve was altered only after the post peak region. Hence, in the present study, the effect of fibers on the bond stress slip response between deformed bar and concrete has not been considered.

It should be noted that, the bond/slip elements have been introduced into the ANSYS [1] FE model from the initial load steps, i.e. prior to cracking. As the strains were quite small at this stage, the effects of the additional stiffness on the overall structural behavior was expected to stiffen the structure marginally. The initiation of cracks and the subsequent sudden softening in the crack normal directions was affected significantly by the presence of these bond/slip elements. The presence of these bond/slip spring elements helped in gradually reducing the load transferred in the cracked elements allowing a stress redistribution to take place in a realistic manner. The stress cut-off behavior has not been considered in this study. The presence of such effects would possibly lead to a better prediction of the total displacements particularly after the peak load.

4. Results and discussions

Table 1 gives results for all the 15 beams tested along with experimental material property data and Table 2 shows the material properties used in FE analysis. Fig. 5(a) and (b) shows the load deflection response obtained from test along with FE results for fully and partially prestressed beams. From the load deflection response, it is clear that the initial portion of the load deflection curve is in close agreement with the experimental findings. Addition of fibers increased the cracking and ultimate strength and reduces the deformational characteristics. As seen from the load deflection curve in Fig. 5, the post peak region was modified due to the addition of fibers. As the load increased, the deflection increased and more fibers in the tensile extremity pulled out across the crack. As further load was applied, the cracks developed in the flexure zone, as a results of which some slip took place and hence a small drop-of in the load was observed (Fig. 5). With further increase in the load up to the peak, the effect of bond (tension-stiffening) was seen. Thereafter due to bond-slip between reinforcement (fiber, prestressing wire, deformed bar) and concrete a sudden drop in the post-peak region was observed.

Fig. 5(a) and (b) also show the load deflection curve obtained from FEM along with experimental curves for partial depth FRC beam specimen A-FPhf/f1-5. From the examination of these load deflection curves, it is seen that FEM load response prediction is close to the experimental results in the working load range. However, as the load reached the peak it is seen that the FEM results are stiffer than the corresponding test results. While initially a bilinear bond slip relationship (Fig. 4) was employed to model the concrete steel interface, it was found that this led to numerical convergence problems. Therefore a linear bond slip relationship (without tension cut-off) was used in the modelling which resulted in the stiffer responses particularly in the post peak region.

From the examination of Fig. 5(a) and (b) and Table 1, 3 and 4 it seen that, both fully/partially prestressed beams, exhibited similar response at all the stages of loading and practically identical results and improvements in the desired structural characteristics were brought about by using the fiber over only half the depth. From an examination of these load deflection curves of both test and FE analysis (Fig. 5(a) and (b)), it is seen that inclusion of fibers, only in half the depth on the tensile side, is effective in bringing about the improvements in the deformational characteristics to almost at par with those obtained with full depth fiber

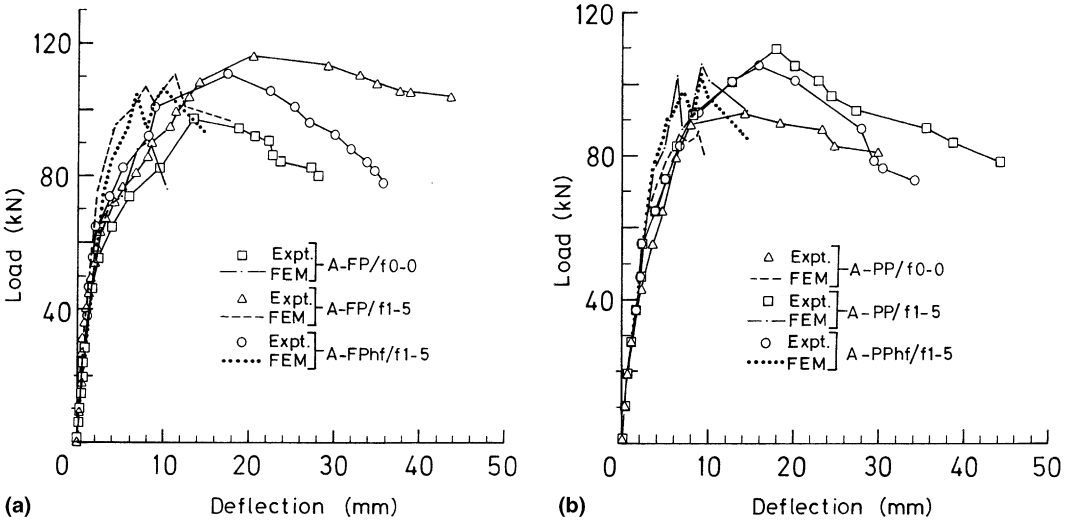

Fig. 5. (a) Load deflection response for fully prestressed beam specimens, (b) load deflection response for partially prestressed beam specimens.

Table 3
Comparison of FEM results at various stages of loading for fully prestressed beam specimens

Beam	Stages	FEM		Expt		FEM/Expt	
		W (kN)	δ (mm)	W (kN)	δ (mm)	W (kN)	δ (mm)
A-FP/f0-0	1	18.10	0.49	19.40	0.59	0.93	0.83
	2	53.13	1.70	55.43	2.68	0.96	0.64
	3	60.33	2.98	64.66	4.47	0.93	0.67
	4	90.49	8.20	96.99	13.50	0.93	0.61
A-FP/f1-5	1	22.10	0.51	23.46	0.62	0.94	0.82
	2	60.30	1.90	64.46	2.63	0.94	0.72
	3	73.70	3.33	78.21	5.26	0.94	0.63
	4	110.50	11.32	117.31	20.55	0.94	0.55
A-FPhf/f1-5	1	21.30	0.56	22.11	0.59	0.96	0.95
	2	60.53	2.38	64.46	2.11	0.94	0.89
	3	71.00	2.90	73.69	3.71	0.96	0.78
	4	106.50	10.50	110.54	17.50	0.96	0.60
A-FPhs/f1-5	1	19.50	0.51	20.29	0.62	0.96	0.82
	2	54.90	1.84	57.95	2.58	0.95	0.72
	3	65.00	3.15	67.65	4.01	0.96	0.79
	4	97.51	9.75	101.47	16.10	0.96	0.61

Table 4
Comparison of FEM results at various stages of loading for partially prestressed beam specimens

Beam	Stages	FEM		Expt		FEM/Expt	
		W (kN)	δ (mm)	W (kN)	δ (mm)	W (kN)	δ (mm)
A-PP/f0-0	1	17.44	0.61	18.33	0.54	0.95	1.13
	2	42.51	2.10	42.78	2.33	0.99	0.90
	3	58.13	2.90	61.10	4.10	0.95	0.71
	4	87.20	8.90	91.65	14.30	0.95	0.62
A-PP/f1-5	1	21.08	0.60	21.93	0.65	0.96	0.92
	2	49.21	2.21	55.43	2.40	0.89	0.92
	3	70.36	3.50	73.09	4.85	0.96	0.73
	4	105.54	9.23	109.63	17.98	0.96	0.52
A-PPhf/f1-5	1	20.45	0.58	21.02	0.63	0.97	0.92
	2	48.77	2.10	55.43	2.13	0.88	0.99
	3	68.15	3.50	70.08	4.70	0.97	0.74
	4	102.23	9.35	105.12	16.00	0.97	0.60
A-PPhs/f1-5	1	18.86	0.64	19.85	0.85	0.95	1.30
	2	44.05	1.81	46.39	1.90	0.95	0.95
	3	62.87	3.00	66.16	4.83	0.95	0.62
	4	94.30	9.43	99.24	20.89	0.95	0.45

beams, from the initial loading stage up to the ultimate load. Full depth fiber inclusion imparts increased ductility and preserves the structural integrity of the members up to the ultimate stage. Table 1, 3, 4 also show the comparison of load deflection response of beams having partial depth fibers over only the shear span. An examination of these Tables reveals that, the cracking load values for these beams were almost the same as in plain concrete beams. As the crack developed in the flexure region due to increase in loads, no fibers came into play to enhance the flexure strength. After the formation of first crack, a small increase of loads were observed due to the effect of fibers in only shear span and it reached its peak and failed in flexure very rapidly.

Table 3 shows the typical finite element results comparison with test results at four stages of loading for the selected beam specimen having no fibers (A-FP/f0-0), 1.5% fiber over full depth and length (A-FP/f1-5), partial

depth fiber ($v_f = 1.5\%$) over full length (A-FPhf/f1-5), and partial depth fibers over only the shear span (A-FPhs/f1-5). The first stage was taken before crack initiation (20% of peak load), the second stage at the initiation of first flexure crack, third stage at a working load level taken to be the peak load/1.5 (load factor), and last stage at peak loading. Table 4 shows the similar comparison of FEM results at four different stages of loading for the partially prestressed beams specimen A-PP/f0-0 (no fibers), A-PP/f1-5 (full depth fibers in full length with $v_f = 1.5\%$) and partial depth fibers over full length (A-PPhf/f1-5) with $v_f = 1.5\%$). From Table 3 and 4 it is seen that, for all the beams, the load and deflection before crack and at first crack in the analysis were very much in agreement with the experimental values. At working load level and at the peak load the values of load obtained from FEM were close to the test results. However, the deflection obtained from FEM was less than those in the test at working load level, first shear crack and at peak. One possible reason for the lower deflection may be due to the fact that linear springs were used to simulate bond slip where as the behavior may be highly nonlinear at these load levels. The ratio of FE analysis to experimental loads ranged from 0.93 to 0.96 for fully prestressed beams and 0.88 to 1.01 for partially prestressed beams at all stages of loading. However, the ratio of deflections predicted by FEM to experimental values at their load levels was found to be in the range of 0.55 to 1.01 in all eight fully prestressed beams and 0.62 to 1.12 for all seven partially prestressed beams at all the load stages.

Figs. 6(a) and 7(a) show the crack pattern obtained at failure for the typical beams tested in this study. The notations shown at various locations shown in Figs. 6(a) and 7(a) have been explained in Table 5. These notations correspond to load levels as indicated in Table 3 and 4. Figs. 6(b) and 7(b) show the crack pattern obtained from FE analysis. In these figures, small dash lines in-

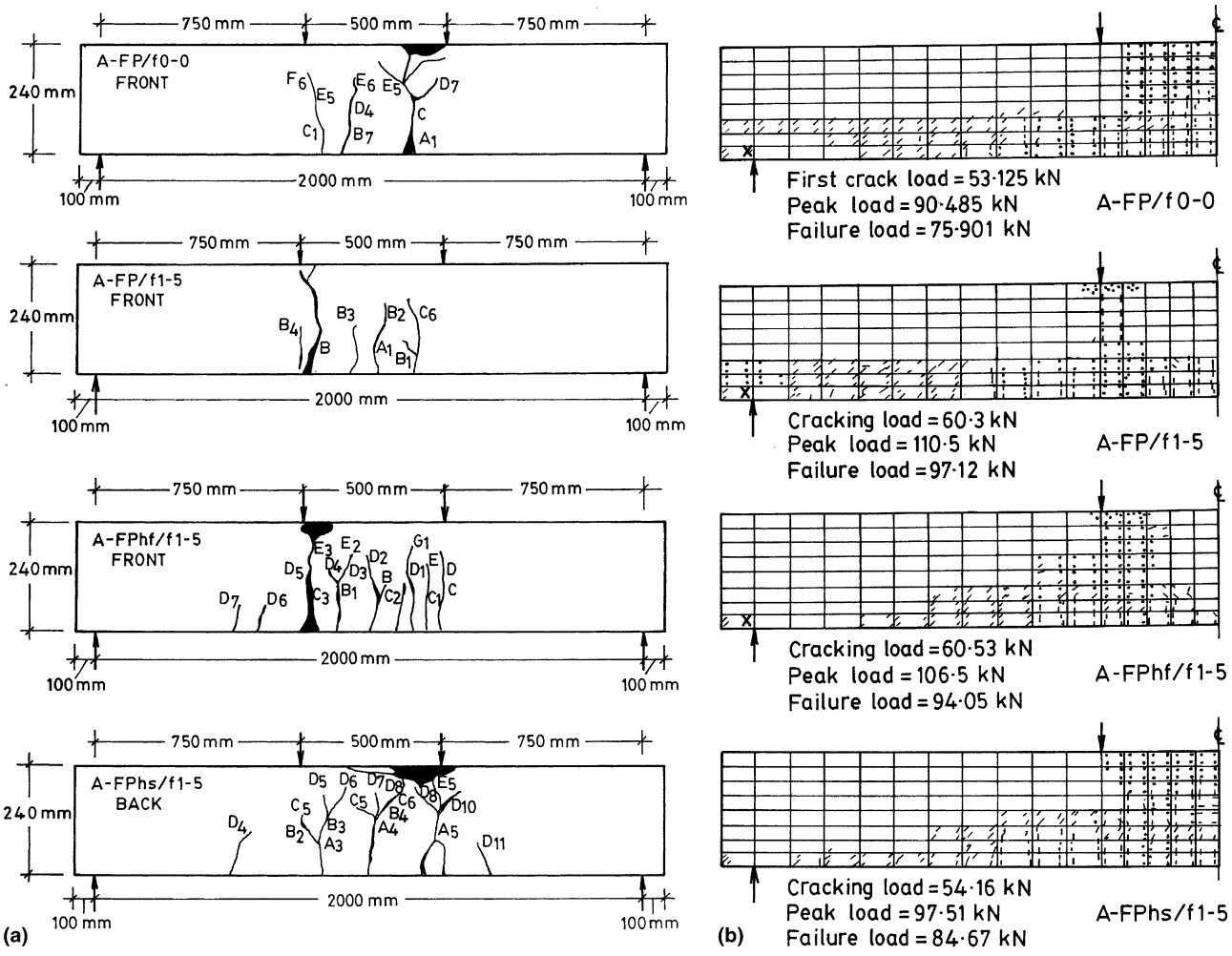

Fig. 6. (a) Experimental observed crack patterns for fully prestressed beams specimens (see Table 5, for notations marked within beams and Table 3 for the corresponding load levels). (b) FEM predicted crack patterns for fully prestressed beam specimens (lines indicate crack orientations and dots indicates crushing of concrete).

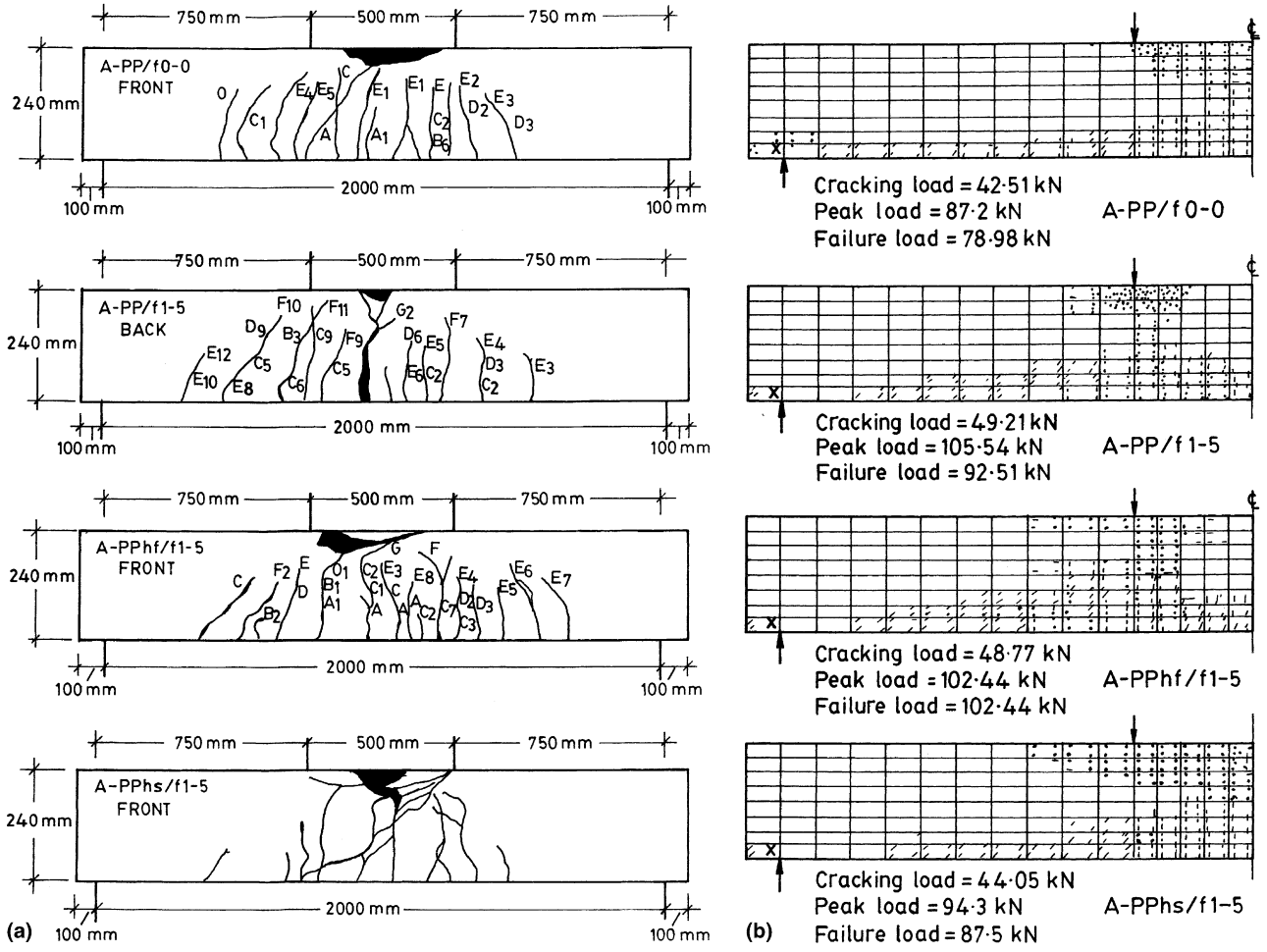

Fig. 7. (a) Experimental Observed Crack Patterns for Partially Prestressed Beams Specimens (see Table 5, for notations marked within beams and Table 4 for the corresponding load levels), (b) FEM Predicted Crack Patterns for Partially Prestressed Beam Specimens (lines indicate crack orientations and dots indicates crushing of concrete).

Table 5
Crack propagation at different load stages

Sl	Beam	$W = P_{cr}$	$P_{cr} \leqslant W \leqslant P_u$	$W > P_u$
1	A-FP/f0-0	A	B,C,D	E,F,G
2	A-FP/f0-5	A	B, C,D,E	F,G,H
3	A-FP/f1-0	A	B,C,D,E,F	G,H
4	A-FP/f1-5	A	B,C,D	F
5	A-FPhf/f1-0	A	B,C,D	E,F,G
6	A-FPhf/f1-5	A	B,C,D	E,F,G
7	A-FPhs/f1-0	A	B,C	D,E
8	A-FPhs/f1-5	A	B,C,D	E,F
9	A-PP/f0-0	A	B,C,D	E,F
10	A-PP/f1-0	A	B,C,D	E,F
11	A-PP/f1-5	A	B,C,D,E	F,G
12	A-PPhf/f1-0	A	B,C,D,E	F,G
13	A-PPhf/f1-5	A	B,C,D,E	F,G
14	A-PPhs/f1-0	A	B,C,D,E	F,G
15	A-PPhs/f1-5	A	B,C,D,E	F,G

Note: The suffix 1–7 after the letter (e.g. A_1, A_2, etc.) in Figs. 6 and 7(a) indicates crack appearance at the same load level A at different locations in the beam.

dicates the crack locations and orientations in each element. The dot (near the loading points) indicates that crushing of concrete takes place in these zones. In both test and analysis, all the first cracks were observed in flexure zone. However, cracks were observed at lower loads in partially prestressed beams as compared fully prestressed beams. As the load increased, the new cracks in both flexure zone and shear span opened, along with propagation of existing cracks. As the load increased these cracks propagated towards the compressive side along with additional cracks in both flexure region and in shear span. At the working load level only about half the total number of cracks that were fully developed at failure were visible, and they were so narrow that for a close look, a magnifying glass was needed to trace them. From the examination of the Figs. 6(a) and (b) and 7(a) and (b) it is clear that, the cracks were more closely spaced in all fiber reinforced prestressed beams at all the stages of loading. The role of fibers is in arresting any advancing cracks and increasing the ductility and post

cracking stiffness of the member right up to failure which results in substantially less deformation than that in plain concrete beams. The number of cracks were consequently less in these beams compared to those in plain concrete prestressed beam as the amount of fiber content increased.

In the case of partially prestressed beam as seen in the crack pattern shown in Fig. 7(a) and (b), the spalling of concrete in the compression side in the flexure span was observed at the failure stages in beams having no fibers, partial depth fibers over full length and only in shear span. In these beams, the flexure cracks reached deep into the compression zone and the available area of concrete in the vicinity of the point of application of the loaded beam was too small to resist the compressive forces and hence these beams failed in crushing. However, in the case of beams having full depth fibers spalling of concrete on compression side was reduced due to the presence of fibers. The inclusion of fibers in fully prestressed beams resulted in higher ultimate strengths as compared to partially prestressed beams. In the case of partially prestressed beams, all the beams exhibited lower cracking load level as compared to fully prestressed beams. Greater deflection was observed under overloads in partially prestressed beams. In the case of partially prestressed beams, failure was due to yielding of deformed steel and spalling of concrete on the compressive side.

5. Conclusions

Based on the comparison of the test results with the FE analysis of 15 fully/partially prestressed beam containing fibers at various locations and varying fibers volume fractions, the following conclusions were drawn:

1. Addition of trough shape steel fiber to high strength concrete, caused an increase of both cracking strength and peak strength. The basic post peak region of the load deflection curve diagram was affected by the addition of fibers. The ascending portion of the load–deflection changed very slightly, but the descending portion became less steep, which resulted in a higher ductility and toughness of the material. The influence of fibers in reducing deformation and increasing flexural capacity was evident even at the failure stage. The fibers were effective in resisting deformation at all stages of loading, from first crack to failure. The maximum increase in flexural strength in fully prestressed beams due to addition of fibers over full depth was found to be 8%, 16%, and 21% for the volume fraction of fiber of 0.5%, 1.0%, and 1.5%, respectively, in these tests.
2. Inclusion of fibers over a partial depth in the tensile side of the prestressed flexural structural members would be economical and lead to considerable cost saving in the design without sacrificing on the desired performance in the area of building elements particularly in precast construction where quality may be maintained. Full depth fiber reinforced members would be necessary in some special structures subject to large strain rates of loading and fatigue. However, inclusion of fiber over half the depth in the shear span, resulted in not much increase in the ultimate load and deformational characteristics when compared to plain concrete beams and is not recommended.
3. The load–deformational characteristics obtained from the finite elements solution was in close agreement with the experimental results at four critical stages of loading. The crack pattern at both initial and at failure stages predicted by FEM was in close agreement with the experiment results, indicating that the effect of fibers on the concrete strength and ductility and its bridging effects in arresting crack propagation have been suitably captured.

References

[1] ANSYS: 5.5. Theory Reference Manual. In: Kohnke P, editor. Elements Reference Manual. 8th ed. September 1998.
[2] Henager CH, Doherty TJ. Analysis of reinforced fibrous concrete beams. Proc ASCE 1976;102(ST1):177–88.
[3] Jenn C, Hong-Jen Y, Hong-Wen C. Behavior of steel fiber reinforced concrete in multi-axial loading. ACI Mater J 1992;89(1):32–40.
[4] Swamy RN, Sa'ad A, Ta'an Al. Deformation and ultimate strength in flexure of reinforced concrete beams made with steel fiber concrete. Proc ACI J 1981;78(5):395–405.
[5] Batson GB, Terry T, Chang MS. Fiber reinforced concrete beam subjected to combined bending and torsion. In: Proceedings of the Fiber Reinforced Concrete International Symposium, Publication SP-81. Detroit, Michigan: ACI; 1984. p. 51–68.
[6] Samir AA, Faisal FW. Flexural behavior of high-strength fiber reinforced concrete beams. ACI Struct J 1993;90(3):279–86.
[7] Samir AA, Khalid M, Faisal FW. Influence of steel fibers and compression reinforcement on deformation of high-strength concrete beams. ACI Struct J 1997;94(6):611–24.
[8] Samer EA, Shiah, TW. Analytical immediate and long-term deflections of fiber reinforced concrete beams. J Struct Eng ASCE 1995;121(4).
[9] Ramzi BAA, Omer QA. Flexural strength of reinforced concrete T-Beams with steel fibers. Cem Concr Compos 1999;21(2):263–8.
[10] Hughes BP. Design of prestressed fiber reinforced concrete beams for impact. ACI J 1981;78(4):276–81.
[11] Narayanan R, Darwish IYS. Shear in prestressed concrete beams containing steel fibers. Int J Cem Compos Lightweight Concr 1987;9(2):81–90.
[12] Balaguru P, Ezildin A. Behavior of partially prestressed beams made with high-strength fiber reinforced concrete. In: Shah SP, Batson editors. Fiber Reinforced Concrete: Properties and Application SP-105. ACI; 1987. p. 419–36.
[13] Kiang-Hwee T, Paramashivam P, Murugappan K. Steel fibers as shear reinforcement in partially prestressed beams. ACI Struct J 1995;92(6):643–52.

[14] Sydney FJ, Joao Bento de H. Prestressed fiber reinforced concrete beams with reduced ratio of shear reinforcement. Cem Concr Compos 1999;21(2):213–21.
[15] Narayanan R, Kareem-Palanjian AS. Torsion in prestressed concrete beams containing steel fibers. Int J Cem Compos Lightweight Concr 1984;6(2):81–91.
[16] Narayanan R, Kareem-Palanjian AS. Torsion bending, and shear in prestressed concrete beams containing steel fibers. ACI J 1986;83(3):423–31.
[17] Faisal FW, Abdul H, Osama FT. Prestressed fiber reinforced concrete beams subjected to torsion. ACI Struct J 1992;89(3):272–83.
[18] Gunashekaran M. The strength and behavior of light weight concrete beams made with fly-ash aggregates and fiber-reinforced partially. Indian Concr J 1975;49(11):332–4.
[19] Sri Ravindrarajah R, Tam ST. Flexural strength of steel fiber reinforced concrete beams. Int J Cem Compos Lightweight Concr 1984;6(4):273–8.
[20] Rahimi MM, Kelser CE. Partially steel-fiber reinforced mortar. J Struct Div ASCE 1979;105(ST1):101–9.
[21] ASCE Task Committee on Concrete and Masonry Structures, ASCE. State of the art report on finite element analysis of reinforced concrete. 1982.
[22] SP-23. Hand Book on Concrete Mixes. Indian Standards Institute; 1982.
[23] Nagaraj TS, Zahida B. Generalization of Abram's Law. Cem Concr Res 1996;26(6):933–42.
[24] Bazant ZP, Cedolin L. Finite element modeling of crack band propagation. J Struct Eng ASCE 1983;109(1):155–77.
[25] Willam KJ, Warnke EP. Constitutive model for the triaxial behavior of concrete. Proc IABSE 1975;19:1–30.
[26] Yin WS, Eric CMS, Thomas MA. Biaxial tests of plain and fiber concrete. ACI Mater J 1998;86(3):236–43.
[27] Parviz S, Cha-Don L. Distribution and orientation of fibers in steel fiber reinforced concrete. ACI Mater J 1990;87(5):433–9.
[28] Naaman AE, Moaven ZF, McGarry FJ. Probabilistic analysis of fiber reinforced concrete. Proc ASCE 1974;100(EM2):397–413.
[29] James PR, James AM. Tensile strength of concrete affected by uniformly distributed and closely spaced short lengths of wire reinforcement. ACI J 1964;61(6):657–70.
[30] George Jr. N, Antoine EN. Bond stress model for fiber reinforced concrete based on bond stress-slip reinforced. ACI Mater J 1989;86(1):45–6.
[31] Edwards AD, Yannopoulos PJ. Local bond-stress to slip relationships for hot rolled deformed bars and mild steel plain bars. ACI J 1979;76(3):228–35.
[32] Spencer RA, Panda AK, Mindess S. Bond of deformed bars in plain and fiber reinforced concrete under reversed cyclic loading. Int J Cem Compos Lightweight Concr 1982;4(1):3–17.